Human Molecular Genetics, 2015, Vol. 24, No. 3 **714–726**
doi:10.1093/hmg/ddu490
Advance Access published on September 30, 2014

Fhl1 W122S causes loss of protein function and late-onset mild myopathy

Valentina Emmanuele[1,4,†], Akatsuki Kubota[1,†], Beatriz Garcia-Diaz[1], Caterina Garone[1], Hasan O. Akman[1], Daniel Sánchez-Gutiérrez[5], Luis M. Escudero[5], Shingo Kariya[2], Shunichi Homma[3], Kurenai Tanji[1,2], Catarina M. Quinzii[1] and Michio Hirano[1,*]

[1]Department of Neurology, [2]Department of Pathology and Cell Biology and [3]Department of Medicine, Columbia University Medical Center, New York, NY 10032, USA, [4]Pediatric Clinic, Istituto di Ricovero e Cura a Carattere Scientifico G. Gaslini, University of Genoa, Genoa 16100, Italy and [5]Departamento de Biología Celular, Universidad de Sevilla and Instituto de Biomedicina de Sevilla (IBiS), Hospital Universitario Virgen del Rocío/CSIC/Universdad de Sevilla, 41013 Seville, Spain

Received July 1, 2014; Revised September 2, 2014; Accepted September 22, 2014

A member of the four-and-a-half-LIM (FHL) domain protein family, FHL1, is highly expressed in human adult skeletal and cardiac muscle. Mutations in *FHL1* have been associated with diverse X-linked muscle diseases: scapuloperoneal (SP) myopathy, reducing body myopathy, X-linked myopathy with postural muscle atrophy, rigid spine syndrome (RSS) and Emery-Dreifuss muscular dystrophy. In 2008, we identified a missense mutation in the second LIM domain of FHL1 (c.365 G>C, p.W122S) in a family with SP myopathy. We generated a knock-in mouse model harboring the c.365 G>C *Fhl1* mutation and investigated the effects of this mutation at three time points (3–5 months, 7–10 months and 18–20 months) in hemizygous male and heterozygous female mice. Survival was comparable in mutant and wild-type animals. We observed decreased forelimb strength and exercise capacity in adult hemizygous male mice starting from 7 to 10 months of age. Western blot analysis showed absence of Fhl1 in muscle at later stages. Thus, adult hemizygous male, but not heterozygous female, mice showed a slowly progressive phenotype similar to human patients with late-onset muscle weakness. In contrast to SP myopathy patients with the FHL1 W122S mutation, mutant mice did not manifest cytoplasmic inclusions (reducing bodies) in muscle. Because muscle weakness was evident prior to loss of Fhl1 protein and without reducing bodies, our findings indicate that loss of function is responsible for the myopathy in the Fhl1 W122S knock-in mice.

INTRODUCTION

Four-and-a half-LIM 1 (FHL1) is a multifunctional protein that is abundant in adult human skeletal and cardiac muscle and widely distributed, albeit at a lower level, in other tissues including brain, placenta, lung, liver, kidney and pancreas (1–3). In mature skeletal muscle, FHL1 has been shown to localize at the I-band and M-line of the sarcomere and participates in sarcomere assembly, muscle growth and differentiation, and biomechanical stress response (4–6). Thus, FHL1 contributes to critical functions in muscle, although its precise roles in these molecular processes have not yet been elucidated.

Considering the high level of FHL1 in skeletal and cardiac muscle, the link between muscle diseases with *FHL1* mutations is not surprising. In humans, >30 mutations in the *FHL1* gene have been identified, in association with: scapuloperoneal (SP) myopathy (7,8); reducing body myopathy with or without rigid spine (9–17); X-linked myopathy with postural muscle atrophy (XMPMA) (18–21); rigid spine syndrome (RSS) (13,17), Emery-Dreifuss muscular dystrophy (16,22,23); contractures, rigid spine and cardiomyopathy (24); left ventricular hypertrophy and contractures (25); hypertrophic cardiomyopathy (HCM) and muscular hypertrophy (16); isolated HCM (26,27) and overlap syndromes (28). FHL1 mutations have been also associated with myofibrillar myopathy pathology (14).

*To whom correspondence should be addressed at: Department of Neurology, Columbia University Medical Center, 630 West 168th Street, P&S 4-423, New York, NY 10032, USA. Tel: +1 2123051048; Fax: +1 2123053986; Email: mh29@cumc.columbia.edu
†The authors wish it to be known that, in their opinion, the first two authors should be regarded as joint first authors.

Structurally, FHL1 is characterized by the tandem arrangement of four-and-a-half-LIM domains (29). LIM domains are cysteine-rich double zinc finger motifs in which cysteine and histidine residues coordinate binding to Zn^{2+} (30). The zinc finger motif mediates protein–protein interactions that allow LIM domain-containing proteins to interact with other LIM domains, tyrosine-containing motifs, PDZ domains, helix–loop–helix domains and ankyrin repeats (31). LIM domains contribute to the targeting of proteins to subcellular domains, which is crucial for protein function (30).

In 2008, in a large Italian-American family with 16 individuals affected by X-linked dominant SP myopathy with hyaline inclusions and vacuoles, we identified a missense mutation (c.365 G>C, p.W122S) affecting the second LIM domain, a hot-spot for FHL1 mutations including W122C, which has been identified in four members of a North European family with SP myopathy (7,8). However, unlike most of the other mutations in the second LIM domain, the W122S/C substitutions do not affect a zinc-binding cysteine or histidine but rather modify the tryptophan adjacent to the histidyl ligand in this domain. This residue, highly conserved in the four LIM domains of FHL1 and across species, has been predicted to be critical for the conformation and stability of the protein, through interactions with neighboring F127, T120 and K102 residues (7).

Scapuloperoneal myopathy owing to the W122S/C substitutions differs from the phenotypes caused by other second LIM domain missense mutations in terms of age-at-onset, severity and progression. Onset of symptoms for affected men is in the second decade of life for the W122S mutation and third decade of life for the W122C substitution, with slow progression to loss of ambulation, respectively, in the third and fifth decade of life, and respiratory insufficiency. Heterozygous women are variably, but less severely, affected by both mutations, with delayed onset of symptoms relative to affected men. Skewed X-inactivation may contribute to the severity of the phenotype in female individuals, together with gender-specific protective/precipitating factors. In contrast to the W122S/C alterations, missense mutations directly affecting the zinc-binding site generally cause RB myopathy with juvenile-onset rapidly progressive severe phenotype in males, and more severe symptoms in female carriers compared with carriers of the W122S/C substitutions (9–11 and 13–16).

To elucidate the role of FHL1 in skeletal muscle and the pathomechanism of *FHL1* mutations, we have generated and characterized a W122S knock-in mouse.

RESULTS

Generation of *Fhl1* knock-in mice

We generated congenic C57BL/6J *Fhl1* knock-in mice using homologous recombination to introduce a c.365G>C *Fhl1* mutation into mouse embryonic stem (ES) cells (Fig. 1A). Homologous recombinants were confirmed by Southern blot analyses using probes recognizing *Fhl1* genomic sequences outside of the targeting vector. Presence of the c.365G>C mutation was confirmed by sequencing (Fig. 1B). Mating of heterozygous female mice and wild-type (WT) male mice produced the expected Mendelian distribution of WT male mice ($Fhl1^{+/y}$), hemizygous male mice ($Fhl1^{p.W122S/y}$), WT female mice ($Fhl1+/+$) and heterozygous female mice ($Fhl1^{p.W122S/+}$) (21 : 32 : 18 : 29%).

Overall phenotype of *Fhl1*$^{p.W122S/y}$ and *Fhl1*$^{p.W122S/+}$ mice

To investigate the role of FHL1 in skeletal and cardiac muscle and the pathomechanism of the *FHL1* p.W122S mutation, we studied hemizygous male mice and heterozygous female mice at three different time points: 3–5 months, 7–10 months and 18–20 months (unless otherwise specified).

Mutant female and male mice had normal birth weight, early growth and lifespans compared with WT animals (Supplementary Material, Fig. S1A). Body weight was comparable in 3- to 5-month-old mutant, females and males, and WT animals; however, starting from 7 to 10 months of age, body weight of hemizygous mutant males was significantly lower than WT animals [WT at 7–10 months: 40.7 ± 2.07 g, mean ± standard deviation (SD); mutants at 7–10 months: 35.1 ± 2.32 g; $P < 0.01$; WT at 18–20 months 43.5 ± 2.74 g; mutants at 18–20 months: 36.7 ± 3.13 g, $P < 0.01$] (Fig. 2A). Nevertheless, body composition assessed by nuclear magnetic resonance imaging (MRI) did not show differences in the proportions of lean tissue, fat and fluid in mutant versus WT animals (Fig. 2B). Heterozygous females did not show any difference in body weight and composition compared with WT animals (Fig. 2A and B).

Skeletal muscle function

To evaluate the effects of the W122S *Fhl1* mutation on skeletal muscle function, we assessed spontaneous locomotor activity by open-field, exercise capacity by rotarod, maximal muscle strength by grip test meter, and long-term exercise by treadmill running test.

Motor function, assessed by rotarod, showed significant decreased latency to fall off the rod in 7- to 10-month-old hemizygous mutant (MUT) animals (30% reduction), compared with WT (47.5 ± 9.4 s, mean ± SD; MUT: 34.6 ± 10.4 s; $P < 0.05$) and in 18- to 20-month-old hemizygous animals (35% reduction), compared with WT (44.3 ± 8.0 s, mean ± SD; MUT: 28.6 ± 9.3 s; $P < 0.05$) (Fig. 2C). Moreover, measurement of the maximal muscle strength by grip test meter using the bar showed significantly decreased strength of forelimbs (30% reduction) in 7- to 10-month-old hemizygous males compared with control animals (WT: 70.2 ± 16.6 g, mean ± SD; MUT: 49.0 ± 23.7 g; $P < 0.05$) (Fig. 2D). The weakness appeared to be restricted to forelimb grip as no difference between mutant and WT animals was observed in combined forelimb and hind limb muscle strength assessed by grid test. Treadmill running studies showed no differences in long-term exercise in mutant versus WT male animals (Supplementary Material, Fig. S1B). Open-field measurement of locomotor activity over 15 min showed no differences in spontaneous horizontal and vertical movements in mutant heterozygous females and hemizygous males compared with WT mice (Supplementary Material, Fig. S1C and D). Heterozygous females did not show any difference in locomotor activity, rotarod performance, muscle strength or treadmill assessments compared with WT animals (data not shown).

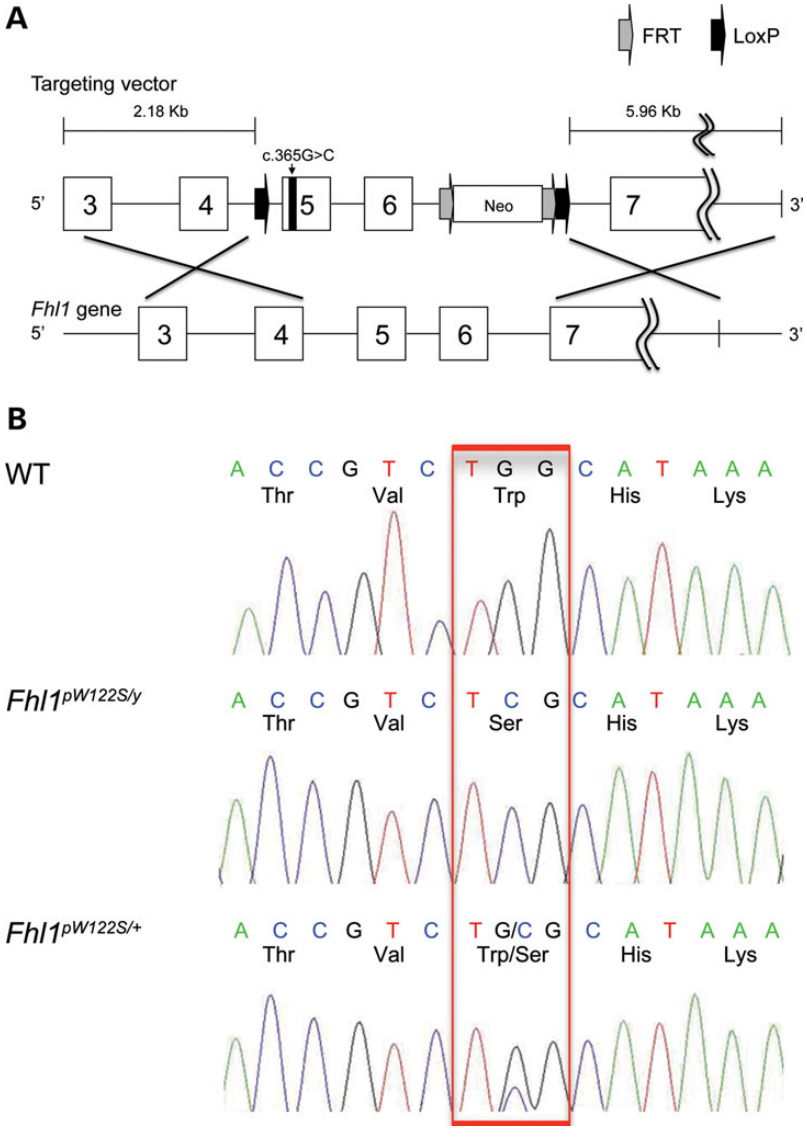

Figure 1. Generation of *Fhl1* knock-in mice. (**A**) Schematic representation of the construct; the cloned region contains a short homology arm extending 2.18 kb to the 5′ end and an long homology arm extending 5.96 kb to the 3′ end. A single lox P site (LoxP) was inserted upstream of *Fhl1* exon 5 (in intron 4), and the LoxP/FRT-flanked neo cassette was inserted downstream of exon 6 (in intron 6). The target region consisted of ∼1.2 kb containing exons 5–6. The c.365G>C mutation (p.W122S) within exon 5 is shown. (**B**) Electropherograms confirming the presence of the mutation in hemizygous male mice ($Fhl1^{pW122S/y}$) and heterozygous female mice ($Fhl1^{pW122S/+}$). WT = wild-type.

To assess muscle damage, we measured plasma creatine kinase (CK) activity at rest. Levels in hemizygous male mice were comparable with WT animals at 3–5 months (WT: 440 ± 273.1 U/L, mean ± SD; MUT: 654.3 ± 280.4 U/L; $P > 0.05$), 7–10 months (WT: 702.7 ± 377.2 U/L, mean ± SD; MUT: 419.3 ± 179.7 U/L; $P > 0.05$) and 18–20 months (WT: 719.3 ± .421.2 U/L, mean ± SD; MUT: 458.9 ± 236.2 U/L; $P > 0.05$).

Cardiac function

We then assessed *Fhl1* mutant mice for a cardiac phenotype by transthoracic echocardiography. No differences were found in hemizygous male mice and heterozygous female mice relative to WTs; in particular, heart rate, fractional shortening (FS%), used to assess left ventricular function, and left ventricular mass index (LVMi) and relative wall thickness (RWT), cardiac hypertrophy, were comparable in WT and mutant animals (Table 1 and Supplementary Material, Table S1).

Impact of W122S mutation on *Fhl1* expression, Fhl1 protein level and localization

The W122S mutation affects a tryptophan conserved in all four LIM domains of Fhl1 protein. Previously, we demonstrated in patients with SP myopathy and the p.W122S mutation that reduction of FHL1 correlated with disease progression, suggesting that the mutation causes instability or misfolding of the protein resulting in loss of FHL1 (7). Therefore, we performed western blots to quantitate levels of Fhl1 in different skeletal muscle groups [triceps, deltoid, distal forelimb flexors (FF), quadriceps, gastrocnemius, tibialis anterior and diaphragm] and in heart of heterozygous and hemizygous

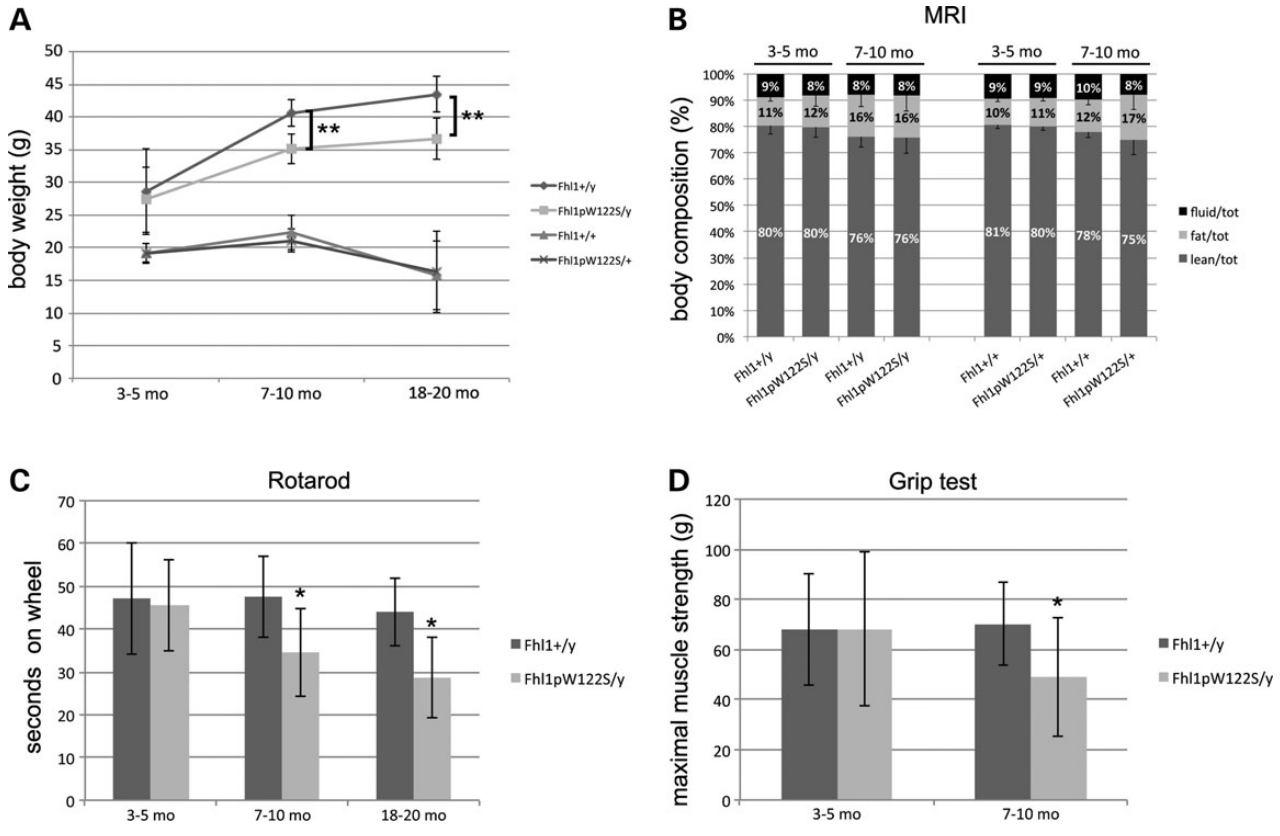

Figure 2. Global phenotype and skeletal muscle function. (**A**) Longitudinal body weight evaluation in hemizygous male mice ($Fhl1^{pW122S/y}$) and heterozygous female mice ($Fhl1^{pW122S/+}$) compared with WT ($Fhl1^{+/y}$ and $Fhl1^{+/+}$); body weight expressed in grams; $^{**}P < 0.01$. (**B**) Magnetic resonance imaging evaluation of body composition expressed as percentage of total body weight in hemizygous male mice ($Fhl1^{pW122S/y}$) and heterozygous female mice ($Fhl1^{pW122S/+}$) compared with WT ($Fhl1^{+/y}$ and $Fhl1^{+/+}$). (**C**) Motor function assessed by Rotarod apparatus in hemizygous male mice ($Fhl1^{pW122S/y}$) compared with WT ($Fhl1^{+/y}$). $^{*}P < 0.05$. (**D**) Measurement of the maximal muscle strength by grip test meter (bar) expressed in grams in hemizygous male mice ($Fhl1^{pW122S/y}$) compared with WT ($Fhl1^{+/y}$). $^{*}P < 0.05$. Analyses were performed at 3–5 months of age (3–5 mo), 7–10 months of age (7–10 mo) and 18–20 months of age (18–20 mo). Data points represent the mean; bars represent SDs.

mice. Levels of Fhl1 were normal in all skeletal muscle groups in hemizygous mutant males at 3–5 months and 10 months of age, with the exception of deltoids, in 10-month-old mutant mice, which showed a significant reduction compared with WT (24 ± 18% residual protein level, mean ± SD; $P < 0.01$). In 20-month-old hemizygous mutant mice, Fhl1 levels were significantly reduced in all muscle groups analyzed, ranging from 0.6 to 6% (2.11% ± 1.68, mean ± SD) residual protein relative to WT muscle (Fig. 3A and B). Levels of Fhl1 in heterozygous female mice were normal in all muscle groups at 10 and 20 months of age compared with WT littermates (data not shown).

We also assessed Fhl1 protein level in heart of 10- and 20-month-old male and female mice and demonstrated a significant reduction in $Fhl1^{p.W122S/y}$ mice at 20 months (23.3 ± 9.9%, mean ± SD; $P < 0.001$) (Fig. 3A).

Interestingly, we also observed reductions in *Fhl1* mRNA expression in skeletal muscle and heart of 20-month-old $Fhl1^{p.W122S/y}$ mice, by a real-time reverse transcriptase–polymerase chain reaction (RT–PCR) assay that detects all Fhl1 transcriptional isoforms (Fig. 3C) (quadriceps 3.71 ± 2.3% of controls, mean ± SD, $P < 0.05$; deltoid 7.6 ± 2.5% of controls, $P < 0.01$; heart 18.6 ± 17.3% of controls, $P < 0.05$). To determine whether there was a qualitative change in the expression pattern of *Fhl1* isoforms, we performed real-time RT–PCR analysis using TaqMan® probe-based primers specific for *Fhl1A*, *Fhl1B* and *Fhl1C* mRNAs. *Fhl1A* transcript was the most abundant isoform in all muscles (Supplementary Material, Fig. S2A). There was no reduction in any of the isoforms at 10 months in skeletal muscle or heart, whereas there were severe reductions of *Fhl1A* and *Fhl1B* mRNAs at 20 months in all analyzed skeletal muscles and heart (Supplementary Material, Fig. S2B and C). Expression of *Fhl1C* was comparable in WT and hemizygous male mice at 10 and 20 months of age in all the analyzed tissues, except deltoid, in 20-month-old mice, which showed a significant 5.6-fold reduction of *Fhl1C* transcript (Supplementary Material, Fig. S2D). *Fhl1* mRNA levels were normal in skeletal and cardiac muscle of heterozygous female mice. Immunofluorescence using antibodies directed against Fhl1 showed normal localization of the protein and confirmed the decreased levels in gastrocnemius and TA muscles of 20-month-old mutant males (Fig. 3D).

Impact of W122S mutation on the expression and protein levels of Fhl1 interacting partners (Mybpc1, 2 and 3)

Since the functional properties of Fhl1 are likely to be mediated by its interacting partners, we studied the effect of mutant *Fhl1*

Table 1. Echocardiographic assessment of cardiac size and function in WT and mutant male mice.

	7–10 months		18–20 months	
	WT ($n = 6$)	MUT ($n = 9$)	WT ($n = 5$)	MUT ($n = 6$)
HR (bpm)	499.8 ± 7.44	498.4 ± 4.98	504.0 ± 2.92	502.2 ± 4.45
Dd (mm)	4.18 ± 0.24	3.95 ± 0.20	3.92 ± 0.28	4.20 ± 0.28
FS (%)	29.4 ± 5.27	34.1 ± 7.07	30.9 ± 2.33	30.9 ± 4.93
DA (mm^2)	14.4 ± 1.42	13.4 ± 1.65	12.6 ± 1.53	15.1 ± 2.39
FAC (%)	46.5 ± 6.65	56.0 ± 8.97	47.9 ± 4.82	47.4 ± 7.27
EDV (μl)	77.8 ± 10.53	68.2 ± 8.34	67.1 ± 12.13	79.1 ± 12.29
ESV (μl)	34.1 ± 8.88	25.1 ± 7.32	27.6 ± 5.60	32.5 ± 6.15
EF (%)	56.6 ± 8.03	63.1 ± 9.99	58.9 ± 3.56	58.5 ± 7.26
LVMi (mg/g)	2.38 ± 0.32	2.62 ± 0.32	2.32 ± 0.54	2.66 ± 0.26
RWT	0.37 ± 0.04	0.37 ± 0.04	0.39 ± 0.02	0.42 ± 0.04

Values represent mean ± SD; WT, wild-type male mice; MUT, hemizygous male mice; HR, heart rate; Dd, diastolic diameter; FS, fractional shortening; DA, diastolic area; FAC, fractional area change; EDV, end-diastolic volume; ESV, end-systolic volume; EF, ejection fraction; LVMi, left ventricular mass index; RWT, relative wall thickness.

on the expression of one of its major interacting proteins, myosin binding protein C (Mybpc) (6). Mybpc has three different isoforms: Mybpc1, mostly expressed in slow-twitch fibers; Mybpc2, mainly expressed in fast-twitch fibers and Mybpc3, expressed in cardiac muscle. We performed western blot analyses of Mybpc1 and Mybpc2 in skeletal muscles of 10- and 20-month-old male mice.

In 10-month-old mice, there was a tendency toward increased Mybpc1 in all investigated muscles of mutant male mice when compared with WT littermates. In 20-month-old mice, the amounts of Mybpc1 were comparable in hemizygous mutant and WT male mice in all muscles. There was a tendency toward decreased Mybpc2 in all muscles of hemizygous mutant male mice at 20 months of age (Supplementary Material, Fig. S3A and B). Protein levels of Mybpc3 in cardiac muscle of 10- and 20-month-old *Fhl1*$^{p.W122S/y}$ mice did not differ from control animals (data not shown). In addition, real-time RT PCR of *Mybpc1* and *Mybpc2* transcripts in 10- and 20-month-old male mice did not identify significant differences in mRNA levels (Supplementary Material, Fig. S3C). Immunofluorescence using antibodies directed against Fhl1 and Mybpc1 showed normal localization of the two proteins in 10-month-old male mice (Supplementary Material, Fig. S3D).

Skeletal and cardiac muscle morphology

Although histological analysis of skeletal muscle (triceps, deltoid, quadriceps, gastrocnemius, tibialis anterior, FF and diaphragm) of hemizygous 3- to 5-month-old males revealed no abnormalities compared with WT littermates, at the age of 10 months, three out of seven hemizygous male mice manifested mild myopathic features characterized by focal reductions of muscle fiber diameter (Fig. 4A–C and I), increased internal nuclei (Fig. 4D and G) and mild fatty replacement (Fig. 4D–F). The abnormalities were not restricted to a specific muscle group. Hematoxylin and eosin (H&E), modified Gomori trichrome and menadione-nitro-blue tetrazolium (NBT) stains did not reveal intracytoplasmic inclusions such as cytoplasmic bodies and reducing bodies (Fig. 4), and the analyses of skeletal muscle of 20-month-old males excluded late development of inclusions. Muscle morphology of heterozygous females did not show any abnormalities (data not shown).

To confirm and quantitate the differences found by conventional morphological analysis and to identify more subtle differences in the muscle of mutant hemizygous male mice, we performed a computerized network-based analysis, recently applied to evaluate the severity of pathology in human neuromuscular diseases (32–34). We analyzed three muscles: (1) Forelimb flexor at 10 months of age, a phenotypically affected muscle, (2) gastrocnemius at 10 months of age, variably involved in conventional morphological studies and (3) gastrocnemius, at 20 months of age, which is biochemically affected with absent Fhl1. Thirty-four characteristics were analyzed: 10 were purely geometrical (e.g. fiber area or the length of the major and minor axes of the fibers), 12 were topological characteristics with a geometrical component (e.g. ratio between the fiber area and adjacent fibers' area) and 12 were topological characteristics that captured information about the organization of the fibers (Supplementary Material, Table S2–S4). In the three analyzed groups, the average size of the mutant fibers appeared slightly smaller than that in the controls (Supplementary Material, Table S2). We then selected the relevant characteristics that better differentiated mutant from WT samples and quantified how well these two groups could be separated in the principal component analysis (PCA) graph using a "PCA Descriptor", which reflects differences between two groups of muscle images (i.e. identical images = 0, poor separation <0.3 and good separation ≥ 1) (35). For comparison of WT and mutant FF images, two geometrical and five topological characteristics were selected. The PCA graph showed two groups of images with partial overlap (Fig. 5B, PCA descriptor = 0.94). In the case of the gastrocnemius, while images from 10-month-old animals were poorly separated based on a combination of geometric and topological characteristics (Fig. 5C, PCA descriptor = 0.40), images from 20-month-old mutants and WTs showed greater separation (Fig. 5D, PCA descriptor = 1.22) with 6 of 7 relevant characteristics containing organizational information. Overall, these findings are consistent with the mild abnormalities revealed by conventional histological characterization of skeletal muscle.

Further analysis of type 1 and type 2 fibers by immunofluorescence-stained sections using primary antibodies against slow myosin isoform did not show any differences in the distribution and number of slow-twitch versus fast-twitch fibers in gastrocnemius at 10 months (percentage of MHC-I-positive fibers: WT 3%; hemizygous male mice 3%) and at 20 months (percentage of MHC-I-positive fibers: WT 2%; hemizygous male mice 2%), and in flexors of the distal forelimb at 10 months (percentage of MHC-I-positive fibers: WT 3%; hemizygous male mice 3%).

Ultrastructural analysis of deltoid and TA of 10-month-old hemizygous male mice did not show significant sarcomere disruption, whereas only a few areas of focal *Z*-line streaming were detected in the deltoid of one mutant mouse (Fig. 6A and B).

Morphological analysis of frozen and formalin-fixed cardiac muscle did not reveal pathologic features in hemizygous male and heterozygous female mice at 3–5, 10 and 20 months (Supplementary Material, Figs S4 and S5).

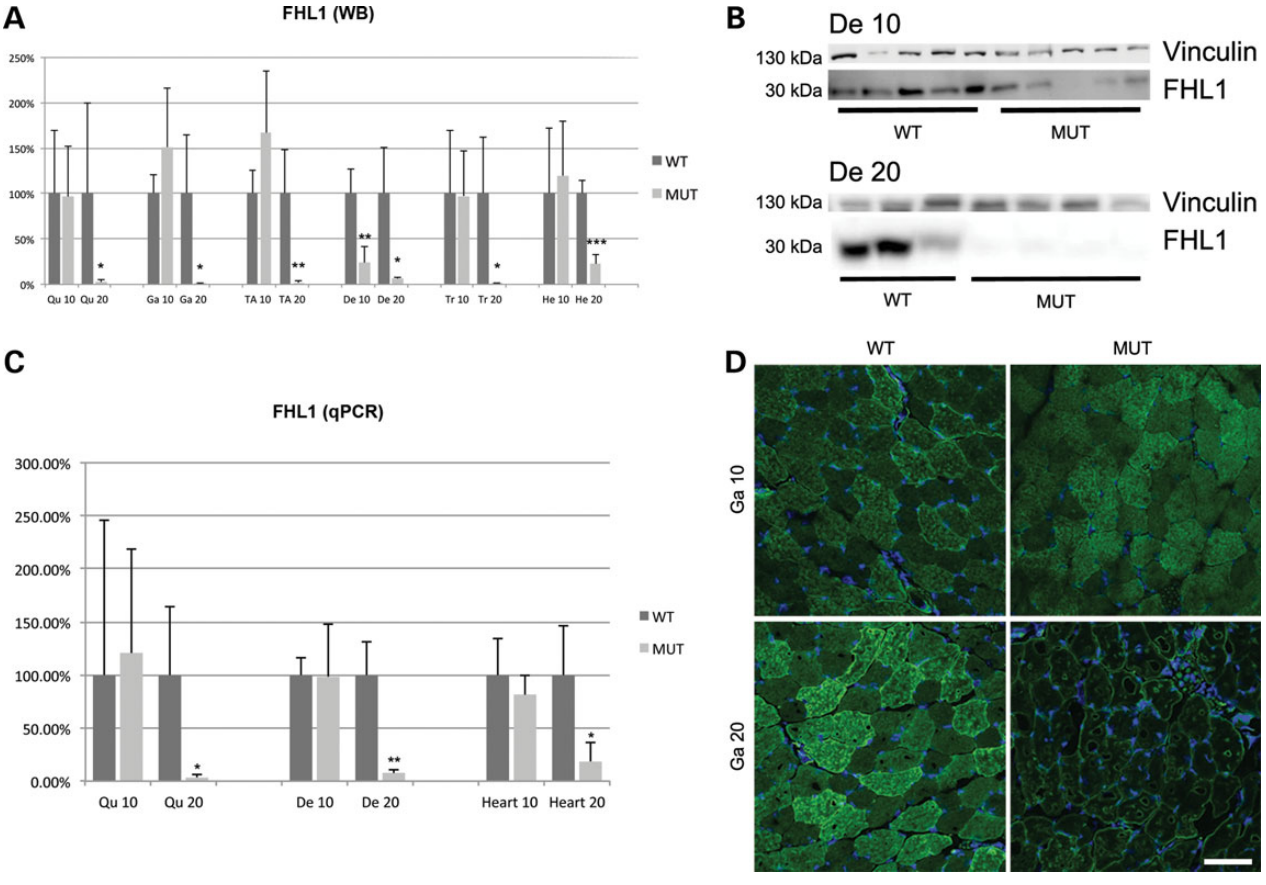

Figure 3. Impact of W122S mutation on Fhl1 expression, protein level and localization. (**A**) Immunoblot analysis of Fhl1 in 10- and 20-month-old WT and mutant (MUT) male mice. Data are expressed as percentage compared with control. Data points represent the mean of at least four animals. Bars represent SDs. Qu, quadriceps; Ga, gastrocnemius; TA, tibialis anterior; De, deltoid; Tr, triceps; He, heart. $^{*}P < 0.05$; $^{**}P < 0.01$; $^{***}P < 0.001$. (**B**) Representative immunoblot of Fhl1 and vinculin in deltoid muscle (De) of hemizygous male mice (MUT) and WT mice at 10 and 20 months of age. WT, wild-type; MUT, mutant. (**C**) Relative percentage of *Fhl1* mRNA expression in mutant male mice (MUT) compared with WT. Data are expressed as mean of at least four animals. Bars represent SDs. Qu, quadriceps; De, deltoid; He, heart. $^{*}P < 0.05$; $^{**}P < 0.01$. (**D**) Composite color images showing nuclear (DAPI, in blue) and Fhl1 (Aviva Systems Biology, in green) immunostaining in WT and mutant (MUT) male mice gastrocnemius at 10 (Ga 10) and 20 (Ga 20) months of age, showing a reduction of the FHL1 stain in 20-month-old mice. Scale bar indicates 75 μm.

Normal citrate synthase activity in skeletal muscle of *Fhl1* mutant mice

To investigate potential alterations in mitochondrial mass in the skeletal muscle of hemizygous mutant male mice, we measured citrate synthase activity, an index of mitochondrial mass, in a predominantly glycolytic muscle (tibialis anterior) and a mixed oxidative and glycolytic muscle (gastrocnemius) at 10 and 20 months. Citrate synthase activity showed trends toward decreases in both muscles of mutant animals at both ages (Supplementary Material, Fig. S6).

DISCUSSION

In this study, we have generated and characterized a novel *Fhl1* knock-in mouse model of the FHL1 p.W122S missense mutation, which causes X-linked SP myopathy (7). We have demonstrated that the mutated murine protein induces a slowly progressive phenotype in mice similar to human patients harboring the homologous mutation. Clinically, *Fhl1* knock-in male mice presented with an adult-onset myopathy, as shown by reduced exercise capacity in rotarod tests and decreased strength of the forelimbs in the grip meter test, which are similar to the clinical manifestations observed in patients. Similar to the SP patients, adult (7- to 10-month-old) mutant male mice relative to WT showed a significant reduction in body weight. However, in contrast to the patients, who displayed progressive and ultimately fatal myopathy, mutant mice showed very slow progression of the disease with minimal phenotypic differences between 7- to 10-month-old and 18- to 20-month-old mice and similar lifespan of mutant and WT animals. Moreover, the pattern of muscle involvement, distal forelimb-specific weakness and normal overall exercise capacity defect, was different from patients who manifested SP distribution at onset and reduced functional capacity. Individuals carrying the p.W122S mutation have also shown muscle wasting, which correlates with the severity of weakness (36), but muscle hypotrophy/atrophy was not observed in the mutant knock-in mice by gross pathological examination or by MRI.

Morphologic analysis of skeletal muscle showed signs of mild chronic myopathy in mutant male mice, including an overall reduction of fiber size, focal areas of increased connective tissue

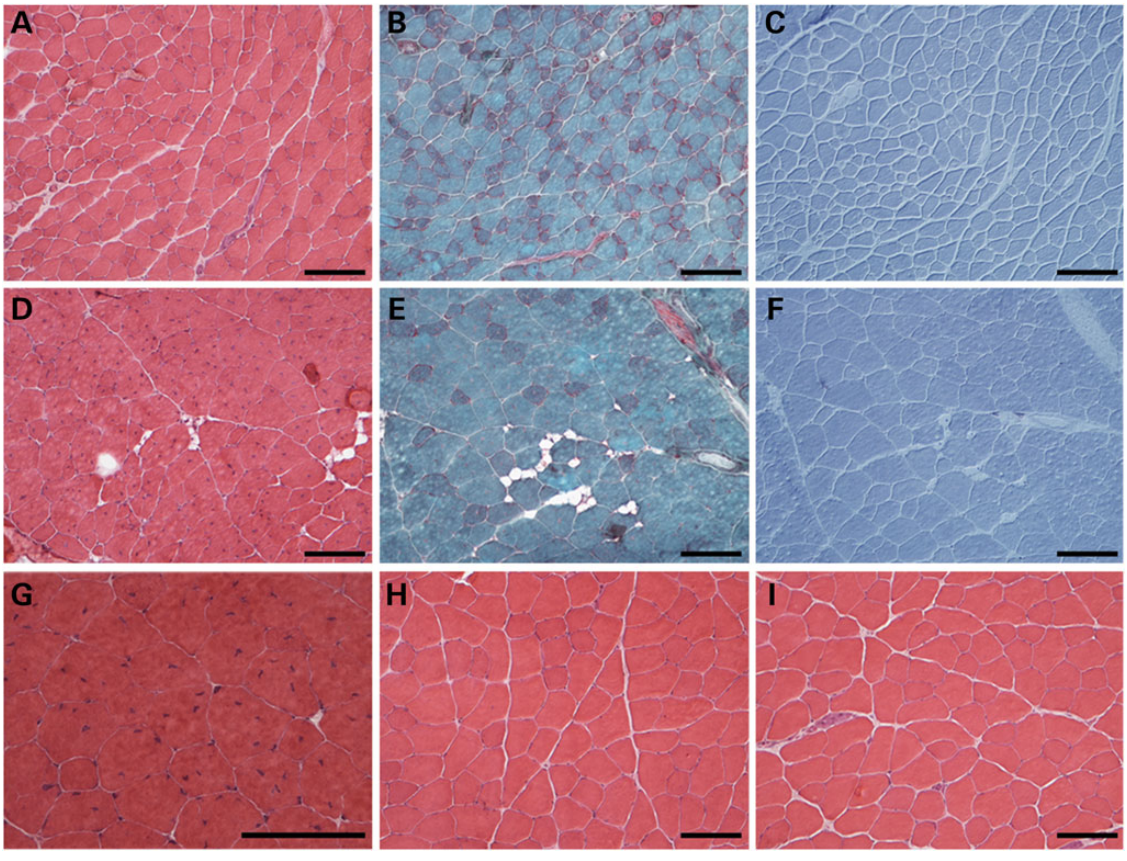

Figure 4. Histological findings in skeletal muscle. (**A**–**C**) Serial cryosections of tibialis anterior of a 10-month-old mutant male mouse compared with WT (**I**), showing an overall reduction of fiber size in the mutant. (**D**–**F**) Serial cryosections of quadriceps of a 10-month-old mutant male mouse compared with WT (**H**), showing a focal area of increased central nuclei and fatty substitution of the muscle. (**G**) Quadriceps of a 10-month-old mutant male mouse at higher magnification, showing increased internal nuclei. (A, D and G–I) Hematoxylin and eosin stain (H&E). (B and E) Modified Gomori trichrome. (C and F) menadione-NBT. Scale bar indicates 100 μm.

and internal nuclei, similar to human muscle pathology. Affected individuals with the p.W122S/C substitutions also showed mild dystrophic changes and elevations of blood CK levels that were not observed in our animal model.

FHL1 mutations in humans have also been associated with variable cardiac involvement including conduction defects, dilated and HCM, and arrhythmias (26). Moreover, *Fhl1*-null mice revealed that absence of Fhl1 blunted cardiac hypertrophic response and preserved cardiac function following pressure overload (5), consistent with a role of Fhl1 as mediator of cardiac hypertrophy, and other studies have revealed increased *FHL1* expression in hypertrophic human hearts (37). In contrast, patients with the p.W122S/C mutations have not manifested structural cardiac abnormalities and similarly our heterozygous female and hemizygous male knock-in mice do not show cardiac functional defects.

The molecular pathomechanism by which mutations in *FHL1* are pathogenic remains unclear. Two non-mutually exclusive hypotheses have been postulated: (1) gain of toxic function, supported by the presence of FHL1 aggregates in the muscle of most of the patients with *FHL1* mutations (including the W122S) and by increased level of the protein in muscle homogenate in some of the patients with RB myopathy (9) and (2) loss of normal protein function via reduced protein level and/or impaired interactions with binding proteins.

Studies in RB myopathy have correlated the severity and the progression of the disease with increased accumulation of RB (9,11). Reducing bodies are intracytoplasmic inclusions that reduce NBT and stain with the menadione-NBT owing to their high sulfhydryl (reducing) content. It has been hypothesized that *FHL1* mutations, especially in the second LIM domain, destabilize the structure of the protein. The misfolded protein accumulates together with other proteins creating aggresome-like intracytoplasmic bodies (9,11,21). It has been proposed that the exposure of nonpolar surface caused by some mutations determines this protein aggregation (8) and that the aggregates have a direct cytotoxic effect.

Recently, Wilding *et al*. (38) showed that overexpression of mutant, but not WT, human FHL1 proteins (including W122S) in C2C12 myoblasts caused impaired myoblast differentiation and formation of protein aggregates analogous to menadione-NBT reducing bodies. In our mouse model, however, mutated p.W122S Fhl1 protein did not produce aggregates. *Z*-line streaming was evident only at the electron microscopy in few areas of deltoid at 10 months of age, and no signs of myofibrillar myopathy or RB were present at the morphological analysis of skeletal muscle. The relatively mild histopathological findings in the muscle of our Fhl1 knock-in mice relative to cultured myoblasts may be attributable to differences in mutant protein level (overexpression versus normal endogenous expression).

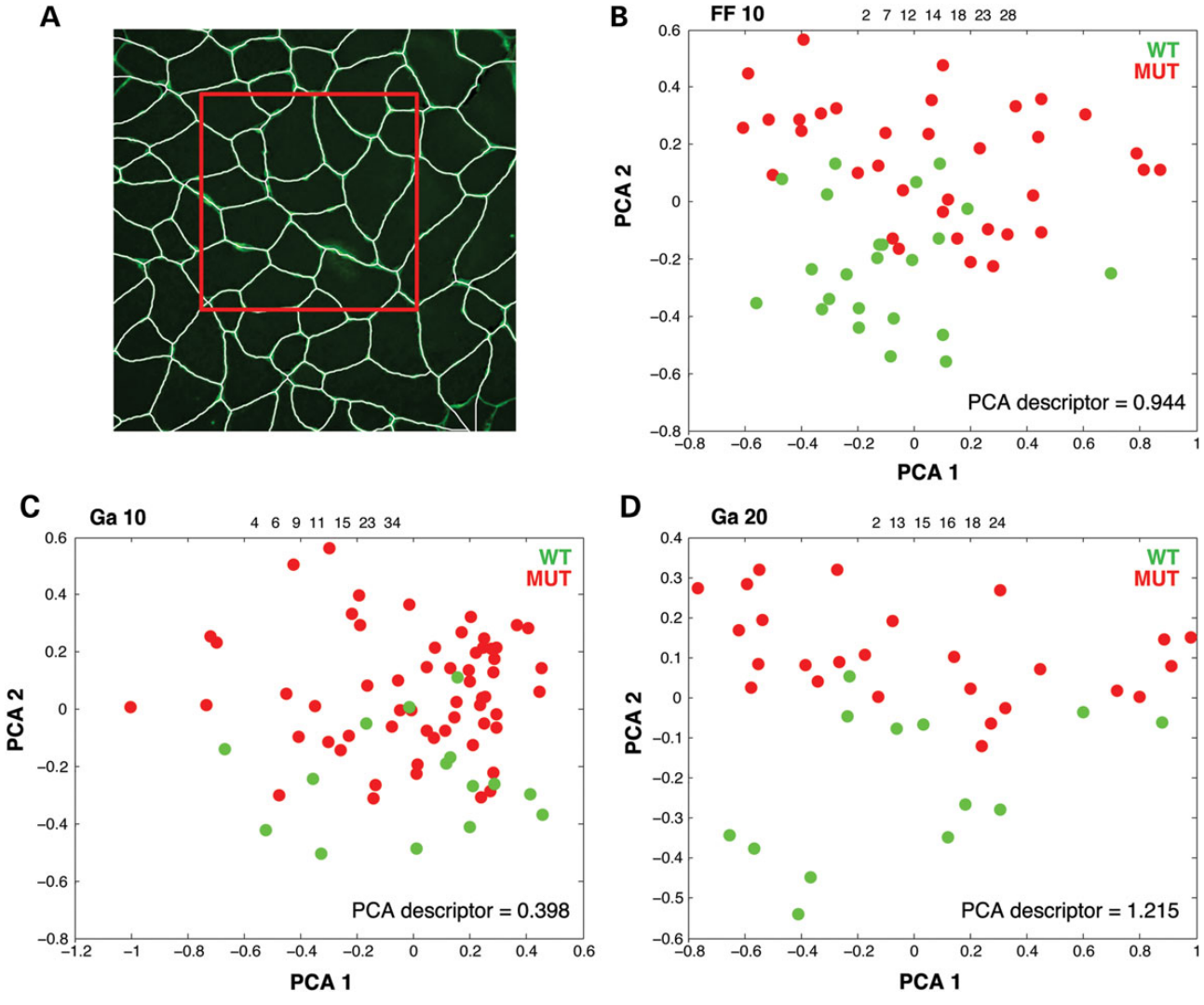

Figure 5. Morphometric analysis of skeletal muscle. (**A**) Representative immunofluorescence of skeletal muscle cryosection showing collagen VI staining in green. The red square indicates the ROI of 1000 × 1000 pixels. (**B**) Principal component analysis in Flexor of distal forelimb at 10 months of age (FF 10) in WT (green dots) and mutant (MUT, red dots) animals showing some overlapping; PCA descriptor = 0.94. (**C**) Principal component analysis in gastrocnemius at 10 months of age (Ga 10) in WT (green dots) and mutant (MUT, red dots) males showing poor separation based on a combination of geometric and topological characteristics; PCA descriptor = 0.398. (**D**) Principal component analysis in gastrocnemius at 20 months of age (Ga 20) in WT (green dots) and mutant (MUT, red dots) males showing better separation than at 10 months of age; PCA descriptor = 1.22. The numbers on the top of the graph in B, C and D indicate the selected relevant characteristics (Supplementary material, Table S2–S4).

Moreover, the absence of RBs in our mice may be due to differences in protein turnover in mice compared with humans. Nevertheless, because patients with the FHL1 p.W122S substitution showed reducing bodies that did not correlate with the severity of the myopathy as they were observed only in a minority of the atrophic fibers (unpublished data), reducing bodies are not major contributors to the pathogenesis of p.W122S FHL1.

Also contrasting to C2C12 cells overexpressing mutant FHL1, patients with SP myopathy showed reductions of FHL1 levels that were inversely related to the duration and severity of the disease at the time of biopsy (7). Decreased protein levels in skeletal muscle were also found in RS syndrome (17), XMPMA (18,19,21), EDMD (22), some RB myopathy patients (10,15) and in one family with contractures, rigid spine and cardiomyopathy (24). Similar to the patients with the phenotypically diverse myopathies with FHL1 mutations, *Fhl1* knock-in mice showed decreased protein level in all analyzed muscles of old animals (20 months of age), and in deltoid at an earlier stage (10 months of age). Because of the absence of reducing bodies in our mouse model, decreased levels of Fhl1 protein cannot be attributed to sequestration in focal aggregates.

The decreased levels of protein suggest a "loss of function" mechanism of W122S protein. Moreover, *Fhl1*-null mice have demonstrated that the loss of Fhl1 protein induces an age-dependent progressive myopathy in mice (39). In addition to skeletal muscle metabolic changes, *Fhl1*-null mice manifested myofibrillary disorganization, but not RB, and had reduced survival rates; therefore, loss of protein produced a more severe phenotype than that of our *Fhl1* knock-in mice. The different genetic backgrounds of the two animal models (e.g. Black

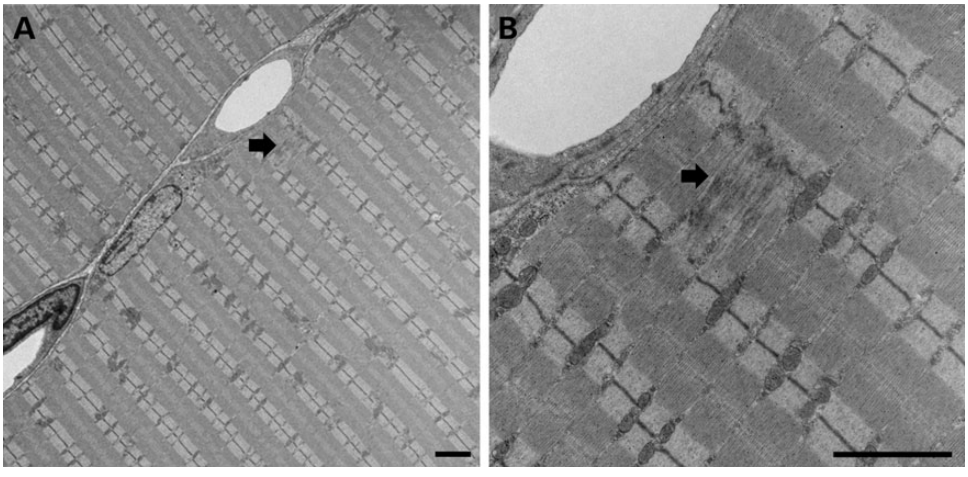

Figure 6. Transmission electron microscopy. (**A** and **B**) Transmission electron micrographs of deltoid in a 10-month-old mutant male mouse showing focal streaming of the *Z*-line (arrow), but overall preservation of the sarcomere structure. Scale bar indicates 2 μm.

Swiss of the published *Fhl1*-null mice versus C57BL/6J of the W122S knock-in mice) may contribute to the divergent phenotypes. Regardless of potential genetic background effects in Fhl1 mutant mice, most of the human *FHL1* mutations are not null defects but rather are missense/in-frame rearrangements and protein levels, even if reduced, are not completely absent.

Importantly, decreases of Fhl1 protein in our mouse model did not precede but rather followed the onset of symptoms and was not associated with a more severe clinical and morphologic phenotype in animals older than 12 months relative to younger mice (except for the subtle difference at the morphological level picked up by the computerized network analysis) indicating that the loss of function of the mutated protein rather than the loss of protein is responsible for the phenotype in our model.

The mutation in the second LIM domain may be responsible for a loss of function of FHL1 protein through impaired interactions with FHL1-binding partners. As previously noted, myopathies owing to *FHL1* mutations have been associated with myofibrillar disarray. However, we could not detect an impaired interaction with Mybpc, one of the major myosin-thick filament-regulatory proteins in muscle (6). Our *Fhl1* knock-in mice showed mild skeletal muscle remodeling with reduced fiber size, without sarcomere disruption, consistent with the role of FHL1 as a regulator of skeletal muscle mass. This remodeling function is also supported by a transgenic mice model overexpressing FHL1 in skeletal muscle, which showed muscle hypertrophy with increased fiber size and increased whole body strength, without sarcomere disruption (4).

In conclusion, our study showed that the missense p.W122S mutation in *Fhl1* induces a late-onset mild myopathy with loss of the protein at advanced ages in hemizygous males. This is the first description of a mutant mouse model of a human *FHL1* mutation. In our mice, loss of protein was not required to induce the myopathy and did not significantly aggravate the mutant phenotype. Moreover, we did not find protein aggregates/reducing bodies in the muscle of the mutant animals indicating that RBs are not required to develop FHL1 myopathy. Heterozygous female mice were unaffected further indicating that Fhl1 W122S-associated loss-of-function alone was sufficient to induce the mild myopathic phenotype, manifesting as an X-linked recessive trait. The paucity of myohistological alterations and the location of the W122S at the protein interacting domain suggest that the mutation may hinder protein interactions leading to mild weakness and subsequent loss of Fhl1. Additional studies are necessary to better understand the normal functions of FHL1 in skeletal muscle and the pathomechanism of *FHL1* mutations in X-linked myopathies.

MATERIALS AND METHODS

Generation of *Fhl1* knock-in mice

A 9.36-kb genomic region containing *Fhl1* exons 3–6 (from C57BL/6J BAC clone RP23: 261L6) was initially subcloned into a ∼2.4-kb pSP72 (Promega) backbone vector using the Red®/ET® homologous recombination-based technique (inGenious Targeting Laboratory, Ronkonkoma, NY, USA). The cloned region contained a short homology arm extending 2.18 kb to the 5′ end and a long homology arm extending 5.96 kb to the 3′ end. A single lox P site was inserted upstream of *Fhl1* exon 5 (in intron 4), and the LoxP/FRT-flanked neo cassette was inserted downstream of exon 6 (in intron 6). The target region consisted of ∼1.2 kb containing exons 5–6. The c.365G>C mutation (p.W122S) within exon 5 was generated by 3-step PCR mutagenesis. The PCR amplicon carrying the point mutation was then used to replace the WT sequence using conventional sub-cloning methods. The targeting vector contained a neomycin selection cassette for retransformation prior to electroporation. The targeting construct was linearized with *AscI* restriction enzyme prior to electroporation into C57BL/6J mouse ES cells. After selection with neomycin, ∼200 resistant clones were isolated and screened by PCR using *Fhl1* primers outside of the targeting sequence with neomycin-resistance gene primers. Homologous recombinants were confirmed by Southern blot analyses using probes recognizing *Fhl1* genomic sequences outside of the targeting vector. Presence of the c.365G>C mutation was confirmed by sequencing. Cells from 2–4 ES clones harboring the homologous recombinants were submitted for injection into C57BL/6J blastocysts and generation of chimeric mutant mice. After obtaining

germline transmission of the mutation, mutant mice were mated with FLP expressing mice to eliminate the neomycin cassette flanked by FLP sites.

Animal care

All experiments were performed according to a protocol approved by the Institutional Animal Care and Use Committee of the Columbia University Medical Center and were consistent with the National Institutes of Health Guide for the Care and Use of Laboratory Animals. Mice were housed and bred according to international standard conditions, with a 12-h light, 12-h dark cycle. Both hemizygous males and heterozygous female mice were studied and compared with age- and gender-matched WT animals.

Muscle and cardiac phenotype was analyzed at three different stages in hemizygous male mice and in heterozygous female mice (3- to 5-month-old mice; 7- to 10-month-old mice; 18- to 20-month-old mice), unless otherwise specified.

Body weight was recorded every 4–6 weeks in all the animals. Mice were sacrificed using rapid asphyxiation with carbon dioxide followed by cervical dislocation. Different muscle groups (triceps, deltoid, quadriceps, gastrocnemius, tibialis anterior, FF and diaphragm) and heart were removed and either frozen in the liquid phase of isopentane, pre-cooled near its freezing point with dry ice, or fixed in 10% neutral buffered formalin and embedded in paraffin using standard procedures, or fixed in 2.5% glutaraldehyde in 0.1 M Sorensen's buffer after perfusion for electron microscopy. Wet heart weight was recorded right after dissection. All the experiments were performed in at least five mice per group, unless otherwise specified.

Nuclear magnetic resonance imaging

Measurements of body composition (lean, fat and fluid percentage of body mass) were assessed by nuclear MRI using a mini-Spec NMR analyzer (Buker, Woodlands, TX, USA).

Locomotor activity

Spontaneous horizontal and vertical movements were measured using metabolic chambers (TSE Systems, Inc., Bad Hamburg, Germany). Whole body mobility and coordination were assessed with an accelerating rotarod performance test (Economex Rotarod, Columbus Instruments). We measured latency to fall off a rod of 3.5 cm of diameter, which was rotating initially at a 4-rpm constant speed for 15 s, followed by a continuous acceleration of 1 rpm/s for a maximum of 60 s. After 60 s without falling, the test was ended. Four mice were tested simultaneously, each mouse being separated from the others by a 30-cm-wide and 60-cm-high opaque plexiglass wall. Three consecutive trials for each animal were evaluated after a training period. Data are expressed as percentage of WT values.

Grip strength test

Measurement of the maximal muscle strength of forelimbs and combined forelimbs and hind limbs was performed using a grip strength meter following manufacturer instructions (Bioseb BP 32025, 13845 Vitrolles cedex France). Briefly, animals were allowed to grasp the grid/bar of the tester and then pulled away from it by the tail until grip was released. The force applied at the moment of release was recorded by the machine as the maximal grip strength. Mice were not trained. Three trials were carried out consecutively using the triangular pull bar (for the forelimbs), and three trials were carried out using the grid (for the four limbs) for each animal.

Treadmill running study

Long-term exercise capacity at the age of 7 to 10 months was assessed in 17 mice (WT males, 3; hemizygous mutant males, 8, WT females, 4; heterozygous females, 2) by a treadmill apparatus (Calo Treadmill, TSE systems, Bad Homburg, Germany). The conveyor belt was set at 0° inclination, a stainless steel grid at the end of the line provided a brief electrical stimulus of 0.2 mA in stimulate mice running and brushes prevented the mice from pinching feet between the grid and treadmill. Mice were trained to the machine by a 10-min warm-up at 1.2 m/min for 3 consecutive days prior to the experiment. On the day of the experiment, the initial speed was 4.8 m/min and speed was then increased by 1 m/min every minute, until a mouse could not be prompted to continue running by moderate electric stimulation and either stayed at the electrode for >5 s or stayed at the electrode for >2 s three consecutive times or spent $>50\%$ of the total experiment time on the grid. We measured total distance they traveled until exhaustion.

Plasma creatine kinase activity

Blood (50–100 μl) was collected in heparinized tubes at rest. Plasma was obtained following centrifugation of the blood at 5000 g for 8 min at room temperature. We used the CK Liquid-UV Test NAC (Stanbio) and followed the manufacturer's protocol for the determination of serum CK activity. Briefly, CK working reagent was prepared and warmed up at 37°C. Samples were added to the reagent and mixed gently. Absorbance was read at 2, 3 and 4 min. The average absorbance per minute multiplied by factor 3376 determined results in U/L.

Cardiac function measurement

Echocardiography was performed using Vevo 770 imaging system (Visual Sonics) equipped with a 30-MHz transducer. Mice were sedated with isoflurane in O_2 and placed on a heating pad (37°C) attached to an electrocardiographic monitor. After the mouse chest was shaved, the transducer was gently placed on it for recordings. Heart rate (bpm), FS (%), diastolic and systolic diameters (mm), ejection fraction (%), end-diastolic volume (μl) and end-systolic volume (μl) were measured in 2D mode and M-mode three times for each mouse (40).

mRNA isolation and quantitative real-time PCR

Total RNA was extracted from frozen muscle using RNeasy Fibrous Tissue Mini Kit® (Qiagen Sciences, Germantown, MD, USA). Complementary DNA was synthesized from the extracted total RNA using SuperScript® VILO™ cDNA Synthesis Kit (Invitrogen, Grand Island, NY, USA). Gene expression levels were measured using Taqman qRT–PCR probes

for the total *FHL1* (mm0420610_mH), *FHL1 and Mybpc* isoforms (Mm00615131_m1 for *Mybpc1*, Mm00525419_m1 for *Mybpc2*) and *GAPDH* (4352339E) as housekeeping gene and using the ABI 7500 Real-Time PCR system (Applied Biosystem, Invitrogen, Foster City, CA, USA). Primers for *FHL1* isoforms were designed using Primer3 software according to the cDNA sequence reported in Genebank (http://www.ncbi.nlm.nig.gov) and recognize isoform-specific exons or exon boundaries. Internal FAM-labeled TaqMan® probes were selected (Supplementary Material, Table S5).

Western blot analyses

Skeletal muscle and heart were dissected and frozen in the liquid phase of isopentane, pre-cooled near its freezing point with dry ice, and extracts were obtained in lysis buffer containing 50 mM Tris–HCl, 150 mM NaCl, 1 mM EDTA and 1% NP-40. Fifty micrograms of whole tissue extracts were electrophoresed in an SDS–12% PAGE gel and transferred to Immunoblot PVDF membranes (Immobilon-P transfer membrane, Millipore). Non-specific sites were blocked for 1 h at room temperature in 5% nonfat milk. Incubation was carried out at 4°C overnight with the following primary antibodies: goat anti-FHL1 polyclonal antibody (AHP2070, AbD Serotec, Kidlington, UK, 1 : 1000); rabbit anti-MYBPC1 antibody (ab124196, Abcam, Cambridge, MA, 1 : 1000), rabbit anti-MYBPC2 antibody (TA306943, OriGene, Rockville, MD, 1 : 1000) and mouse anti-vinculin antibody (ab18058, Abcam, 1 : 500). Anti-FHL1 antibody recognizes the amino acid sequence CNKRFVFHNEQVY, in the fourth LIM domain. Protein–antibody interaction was detected by peroxidase-conjugated mouse antibody, peroxidase-conjugated rabbit antibody or peroxidase-conjugated goat antibody using ECL Prime Western Blotting Detection Reagents® (GE Healthcare, Buckinghamshire, UK). Images of the membranes were taken by G:BOX Chemi IR6® (SYNGENE, Cambridge, UK). Quantification of bands intensities was carried out using NIH imageJ 1.44o software.

Histology

To evaluate structural alterations, 5-μm sections of formalin-fixed, paraffin-embedded skeletal and heart muscle were stained with hematoxylin and eosin (H&E) and Masson's trichrome following standard protocols. Eight-micrometer-thick frozen sections of the dissected skeletal muscle groups and heart were cut in a cryostat and stained with H&E, modified Gomori trichrome, menadione-NBT and NADH-tetrazolium reductase (NADH-TR) following standard protocols (41).

Skeletal muscle morphometry

Fiber typing and the amount of collagen in skeletal muscle were determined by immunofluorescence on 8-μm-thick unfixed frozen sections using the following primary antibodies: mouse anti-myosin heavy chain slow (MHCs) antibody (NCL-MHCs, Leica, Newcastle, United Kingdom, 1 : 200) and rabbit anti-collagen type VI antibody (AB7821, Millipore, Temecula, CA, USA, 1 : 300). Images were obtained using a Nikon Eclipse 80i fluorescence microscope (Nikon, Tokyo, Japan) equipped with a Spot Flex digital camera (Diagnostic Instrument, Starling Heights, MI, USA) and analyzed through a digital image-processing algorithm as previously described (34). From the total image (4080 × 4080 pixels), a region of interest (ROI) of 1000 × 1000 pixels was selected. Specifically, our database consisted of FF in 10-month-old male mice, 23 ROI selected from 15 WT images and 35 ROI selected from 27 mutant images; gastrocnemius in 10-month-old male mice, 15 ROI selected from 15 WT images and 59 ROI selected from 44 mutant images; gastrocnemius in 20-month-old male mice, 13 ROI selected from 10 WT images and 26 ROI selected from 16 mutant images. To build the network, we followed the same method described in Sáez *et al*. (2013) (34) with only one modification: a radius $r = 10$ was used to identify the neighbors of each fiber. In this case, 34 characteristics were computed (Supplementary material, Table S2–S4). We used an algorithm based on PCA to select the more relevant characteristics that distinguish two sets of data points and to evaluate the final separation between the two groups (35).

Immunofluorescence

FHL1 and MYBPC1 localization in skeletal muscle was detected by immunofluorescence on 8-μm-thick frozen sections fixed in ice-cold acetone for 10 min, rinsed and incubated overnight with blocking solution (PBS, 10% Triton X and 300 mg BSA) at 4°C. The slides were subsequently incubated overnight at 4°C with rabbit polyclonal anti-FHL1 antibody, C-terminal region (ARP34378 T100, Aviva Systems Biology, San Diego, CA, USA, 1 : 100) and Mybpc1 (Developmental Studies Hybridoma Bank, ALD66, 0.6 μg/ml), and then with Alexa Fluor®-conjugated secondary antibody 488 goat anti-rabbit and Alexa Fluor®-conjugated secondary antibody 594 goat anti-mouse at room temperature for 1 h (A11034 and A11005, Molecular Probes by Life Technologies, Carlsbad, CA, USA, 1 : 1000), with or without DAPI for nuclear staining. Sections were imaged using an SP5 Leica confocal microscope (Leica Microsystems, Wetzlar, Germany).

Citrate synthase activity in skeletal muscle

To measure activity of mitochondrial citrate synthase, 10–40 mg of skeletal muscle (gastrocnemius and TA of 10-month-old mice and 20-month-old mice) were homogenized in CPT medium (0.05 M Tris–HCl and 0.15 M KCl, pH 7.5). The homogenates were then centrifuged at 2500 rpm (9.5 g) for 20 min at 4°C. The supernatant was used for both enzymatic assay and protein quantification. The enzymatic assay measured the reduction of 1 mM 5,5′ dithiobis(2-nitrobenzoic acid) in 1 M Tris–HCl pH 8.1 at 412 nm, at 30°C for 2 min in the presence of the sample, 10 mM acetyl-CoA and 10 mM oxalacetic acid. Citrate synthase activity was normalized to protein content and expressed in μmol/min/mg protein.

Transmission electron microscopy on tissue

Tissue was fixed with 2.5% glutaraldehyde in 0.1 M Sorenson's buffer (pH 7.2). Tissue was then post-fixed with 1% OsO4 also in Sorenson's buffer for 1 h. After dehydration, tissue was embedded in Lx-112 (Ladd Research Industries, Inc.). Thin sections were cut on the MT-7000 ultramicrotome at 60 nm thick. The sections were stained with uranyl acetate and lead citrate and

examined under a JEOL JEM-1200 EXII electron microscope. Images were captured with an ORCA-HR digital camera (Hamamatsu) and recorded with an AMT Image Capture Engine.

Statistical analysis

Data are expressed as mean ± SD of at least five animals per group, unless otherwise specified. Statistical analyses were performed using the unpaired Student's *t*-test or the one-way analysis of variance with Bonferroni's multiple comparison. A *P*-value of <0.05 was considered to be statistically significant.

A power calculation was performed for FS as it was the parameter of greatest scientific interest in the echocardiography data using a two-sample *t*-test. Powering for a 40% effect size gave 93.8% power at alpha level of 0.025 (using a Bonferroni adjustment assuming the analysis was confined to two outcomes) for the 7- to 10-month male mice ($n = 6$ for WT and $n = 9$ for MUT) and 83.6% power at alpha level of 0.025 for the 18- to 20-month-old male mice ($n = 5$ for WT and $n = 6$ for MUT).

SUPPLEMENTARY MATERIAL

Supplementary Material is available at *HMG* online.

ACKNOWLEDGEMENTS

We are grateful to Dr Kristy R Brown from the Department of Pathology, Columbia University Medical Center, NY, for her assistance with the preparation and analysis of the electron microscopic sections, to Dr Antoine Muchir from the Department of Medicine Cardiology, Columbia University Medical Center, for his assistance with cardiac evaluation of the mice and to Dr Joshua F Kriger from the Department of Biostatistics, Mailman School of Public Health, Columbia University Medical Center, for his assistance with statistical analyses.

Conflict of Interest statement. None declared.

FUNDING

This work has been supported by the Muscular Dystrophy Association (MDA), grant number 115567; and by the Caffarelli Family Study Research (CSFR) Foundation, Inc. L.M.E. and D.S.-G. are supported by the Ramón y Cajal program (PI13/01347), and the Spanish government grants: BFU2011-25734 and PI13/01347.

REFERENCES

1. Lee, S.M., Tsui, S.K., Chan, K.K., Garcia-Barcelo, M., Waye, M.M., Fung, K.P., Liew, C.C. and Lee, C.Y. (1998) Chromosomal mapping, tissue distribution and cDNA sequence of four-and-a-half LIM domain protein 1 (FHL1). *Gene*, **216**, 163–170.
2. Greene, W.K., Baker, E., Rabbitts, T.H. and Kees, U.R. (1999) Genomic structure, tissue expression and chromosomal location of the LIM-only gene, SLIM1. *Gene*, **232**, 203–207.
3. Lee, S.M., Li, H.Y., Ng, E.K., Or, S.M., Chan, K.K., Kotaka, M., Chim, S.S., Tsui, S.K., Waye, M.M., Fung, K.P. *et al.* (1999) Characterization of a brain-specific nuclear LIM domain protein (FHL1B) which is an alternatively spliced variant of FHL1. *Gene*, **237**, 253–263.
4. Cowling, B.S., McGrath, M.J., Nguyen, M.A., Cottle, D.L., Kee, A.J., Brown, S., Schessl, J., Zou, Y., Joya, J., Bonnemann, C.G. *et al.* (2008) Identification of FHL1 as a regulator of skeletal muscle mass: implications for human myopathy. *J. Cell. Biol.*, **183**, 1033–1048.
5. Sheikh, F., Raskin, A., Chu, P.H., Lange, S., Domenighetti, A.A., Zheng, M., Liang, X., Zhang, T., Yajima, T., Gu, Y. *et al.* (2008) An FHL1-containing complex within the cardiomyocyte sarcomere mediates hypertrophic biomechanical stress responses in mice. *J. Clin. Invest.*, **118**, 3870–3880.
6. McGrath, M.J., Cottle, D.L., Nguyen, M.A., Dyson, J.M., Coghill, I.D., Robinson, P.A., Holdsworth, M., Cowling, B.S., Hardeman, E.C., Mitchell, C.A. *et al.* (2006) Four and a half LIM protein 1 binds myosin-binding protein C and regulates myosin filament formation and sarcomere assembly. *J. Biol. Chem.*, **281**, 7666–7683.
7. Quinzii, C.M., Vu, T.H., Min, K.C., Tanji, K., Barral, S., Grewal, R.P., Kattah, A., Camano, P., Otaegui, D., Kunimatsu, T. *et al.* (2008) X-linked dominant scapuloperoneal myopathy is due to a mutation in the gene encoding four-and-a-half-LIM protein 1. *Am. J. Hum. Genet.*, **82**, 208–213.
8. Chen, D.H., Raskind, W.H., Parson, W.W., Sonnen, J.A., Vu, T., Zheng, Y., Matsushita, M., Wolff, J., Lipe, H. and Bird, T.D. (2010) A novel mutation in FHL1 in a family with X-linked scapuloperoneal myopathy: phenotypic spectrum and structural study of FHL1 mutations. *J. Neurol. Sci.*, **296**, 22–29.
9. Schessl, J., Zou, Y., McGrath, M.J., Cowling, B.S., Maiti, B., Chin, S.S., Sewry, C., Battini, R., Hu, Y., Cottle, D.L. *et al.* (2008) Proteomic identification of FHL1 as the protein mutated in human reducing body myopathy. *J. Clin. Invest.*, **118**, 904–912.
10. Shalaby, S., Hayashi, Y.K., Nonaka, I., Noguchi, S. and Nishino, I. (2009) Novel FHL1 mutations in fatal and benign reducing body myopathy. *Neurology*, **72**, 375–376.
11. Schessl, J., Taratuto, A.L., Sewry, C., Battini, R., Chin, S.S., Maiti, B., Dubrovsky, A.L., Erro, M.G., Espada, G., Robertella, M. *et al.* (2009) Clinical, histological and genetic characterization of reducing body myopathy caused by mutations in FHL1. *Brain*, **132**, 452–464.
12. Astrea, G., Schessl, J., Clement, E., Tosetti, M., Mercuri, E., Rutherford, M., Cioni, G., Bonnemann, C.G., Muntoni, F. and Battini, R. (2009) Muscle MRI in FHL1-linked reducing body myopathy. *Neuromuscul. Disord.*, **19**, 689–691.
13. Schessl, J., Columbus, A., Hu, Y., Zou, Y., Voit, T., Goebel, H.H. and Bonnemann, C.G. (2010) Familial reducing body myopathy with cytoplasmic bodies and rigid spine revisited: identification of a second LIM domain mutation in FHL1. *Neuropediatrics*, **41**, 43–46.
14. Selcen, D., Bromberg, M.B., Chin, S.S. and Engel, A.G. (2011) Reducing bodies and myofibrillar myopathy features in FHL1 muscular dystrophy. *Neurology*, **77**, 1951–1959.
15. Schreckenbach, T., Henn, W., Kress, W., Roos, A., Maschke, M., Feiden, W., Dillmann, U., Schulz, J.B., Weis, J. and Claeys, K.G. (2013) Novel FHL1 mutation in a family with reducing body myopathy. *Muscle Nerve*, **47**, 127–134.
16. Malfatti, E., Olive, M., Taratuto, A.L., Richard, P., Brochier, G., Bitoun, M., Gueneau, L., Laforet, P., Stojkovic, T., Maisonobe, T. *et al.* (2013) Skeletal muscle biopsy analysis in reducing body myopathy and other FHL1-related disorders. *J. Neuropathol. Exp. Neurol.*, **72**, 833–845.
17. Shalaby, S., Hayashi, Y.K., Goto, K., Ogawa, M., Nonaka, I., Noguchi, S. and Nishino, I. (2008) Rigid spine syndrome caused by a novel mutation in four-and-a-half LIM domain 1 gene (FHL1). *Neuromuscul. Disord.*, **18**, 959–961.
18. Windpassinger, C., Schoser, B., Straub, V., Hochmeister, S., Noor, A., Lohberger, B., Farra, N., Petek, E., Schwarzbraun, T., Ofner, L. *et al.* (2008) An X-linked myopathy with postural muscle atrophy and generalized hypertrophy, termed XMPMA, is caused by mutations in FHL1. *Am. J. Hum. Genet.*, **82**, 88–99.
19. Schoser, B., Goebel, H.H., Janisch, I., Quasthoff, S., Rother, J., Bergmann, M., Muller-Felber, W. and Windpassinger, C. (2009) Consequences of mutations within the C terminus of the FHL1 gene. *Neurology*, **73**, 543–551.
20. Binder, J.S., Weidemann, F., Schoser, B., Niemann, M., Machann, W., Beer, M., Plank, G., Schmidt, A., Bisping, E., Poparic, I. *et al.* (2012) Spongious hypertrophic cardiomyopathy in patients with mutations in the four-and-a-half LIM domain 1 gene. *Circ. Cardiovasc. Genet.*, **5**, 490–502.
21. Feldkirchner, S., Walter, M.C., Muller, S., Kubny, C., Krause, S., Kress, W., Hanisch, F.G., Schoser, B. and Schessl, J. (2013) Proteomic characterization of aggregate components in an intrafamilial variable FHL1-associated myopathy. *Neuromuscul. Disord.*, **23**, 418–426.

22. Gueneau, L., Bertrand, A.T., Jais, J.P., Salih, M.A., Stojkovic, T., Wehnert, M., Hoeltzenbein, M., Spuler, S., Saitoh, S., Verschueren, A. *et al.* (2009) Mutations of the FHL1 gene cause Emery-Dreifuss muscular dystrophy. *Am. J. Hum. Genet.*, **85**, 338–353.
23. Tiffin, H.R., Jenkins, Z.A., Gray, M.J., Cameron-Christie, S.R., Eaton, J., Aftimos, S., Markie, D. and Robertson, S.P. (2013) Dysregulation of FHL1 spliceforms due to an indel mutation produces an Emery-Dreifuss muscular dystrophy plus phenotype. *Neurogenetics*, **14**, 113–121.
24. Knoblauch, H., Geier, C., Adams, S., Budde, B., Rudolph, A., Zacharias, U., Schulz-Menger, J., Spuler, A., Yaou, R.B., Nurnberg, P. *et al.* (2010) Contractures and hypertrophic cardiomyopathy in a novel FHL1 mutation. *Annal. Neurol.*, **67**, 136–140.
25. Gossios, T.D., Lopes, L.R. and Elliott, P.M. (2013) Left ventricular hypertrophy caused by a novel nonsense mutation in FHL1. *Eur. J. Med. Genet.*, **56**, 251–255.
26. Hartmannova, H., Kubanek, M., Sramko, M., Piherova, L., Noskova, L., Hodanova, K., Stranecky, V., Pristoupilova, A., Sovova, J., Marek, T. *et al.* (2013) Isolated X-linked hypertrophic cardiomyopathy caused by a novel mutation of the four-and-a-half LIM domain 1 gene. *Circ. Cardiovasc. Genet.*, **6**, 543–551.
27. Friedrich, F.W., Wilding, B.R., Reischmann, S., Crocini, C., Lang, P., Charron, P., Muller, O.J., McGrath, M.J., Vollert, I., Hansen, A. *et al.* (2012) Evidence for FHL1 as a novel disease gene for isolated hypertrophic cardiomyopathy. *Hum. Mol. Genet.*, **21**, 3237–3254.
28. Sarkozy, A., Windpassinger, C., Hudson, J., Dougan, C.F., Lecky, B., Hilton-Jones, D., Eagle, M., Charlton, R., Barresi, R., Lochmuller, H. *et al.* (2011) Phenotypic heterogeneity in British patients with a founder mutation in the FHL1 gene. *Eur. J. Hum. Genet.*, **19**, 1038–1044.
29. Morgan, M.J., Madgwick, A.J., Charleston, B., Pell, J.M. and Loughna, P.T. (1995) The developmental regulation of a novel muscle lim-protein. *Biochem. Biophys. Res. Commun.*, **212**, 840–846.
30. Kadrmas, J.L. and Beckerle, M.C. (2004) The LIM domain: from the cytoskeleton to the nucleus. *Nat. Rev. Mol. Cell. Biol.*, **5**, 920–931.
31. Shathasivam, T., Kislinger, T. and Gramolini, A.O. (2010) Genes, proteins and complexes: the multifaceted nature of FHL family proteins in diverse tissues. *J. Cell. Mol. Med.*, **14**, 2702–2720.
32. Escudero, L.M., Costa Lda, F., Kicheva, A., Briscoe, J., Freeman, M. and Babu, M.M. (2011) Epithelial organisation revealed by a network of cellular contacts. *Nat. Commun.*, **2**, 526.
33. Saez, A., Acha, B., Montero-Sanchez, A., Rivas, E., Escudero, L.M. and Serrano, C. (2013) Neuromuscular disease classification system. *J. Biomed. Opt.*, **18**, 066017.
34. Saez, A., Rivas, E., Montero-Sanchez, A., Paradas, C., Acha, B., Pascual, A., Serrano, C. and Escudero, L.M. (2013) Quantifiable diagnosis of muscular dystrophies and neurogenic atrophies through network analysis. *BMC Med.*, **11**, 77.
35. Sanchez-Gutierrez, D., Saez, A., Pascual, A. and Escudero, L.M. (2013) Topological progression in proliferating epithelia is driven by a unique variation in polygon distribution. *PLoS One*, **8**, e79227.
36. Wilhelmsen, K.C., Blake, D.M., Lynch, T., Mabutas, J., De Vera, M., Neystat, M., Bernstein, M., Hirano, M., Gilliam, T.C., Murphy, P.L. *et al.* (1996) Chromosome 12-linked autosomal dominant scapuloperoneal muscular dystrophy. *Ann. Neurol.*, **39**, 507–520.
37. Cowling, B.S., Cottle, D.L., Wilding, B.R., D'Arcy, C.E., Mitchell, C.A. and McGrath, M.J. (2011) Four and a half LIM protein 1 gene mutations cause four distinct human myopathies: a comprehensive review of the clinical, histological and pathological features. *Neuromuscul. Disord.*, **21**, 237–251.
38. Wilding, B.R., McGrath, M.J., Bonne, G. and Mitchell, C.A. (2014) FHL1 mutations that cause clinically distinct human myopathies form protein aggregates and impair myoblast differentiation. *J. Cell. Sci*, **127**, 2269–2281.
39. Domenighetti, A.A., Chu, P.H., Wu, T., Sheikh, F., Gokhin, D.S., Guo, L.T., Cui, Z., Peter, A.K., Christodoulou, D.C., Parfenov, M.G. *et al.* (2014) Loss of FHL1 induces an age-dependent skeletal muscle myopathy associated with myofibrillar and intermyofibrillar disorganization in mice. *Hum. Mol. Genet.*, **23**, 209–225.
40. Muchir, A., Wu, W., Choi, J.C., Iwata, S., Morrow, J., Homma, S. and Worman, H.J. (2012) Abnormal p38alpha mitogen-activated protein kinase signaling in dilated cardiomyopathy caused by lamin A/C gene mutation. *Hum. Mol. Genet.*, **21**, 4325–4333.
41. Dubowitz, V. and Sewry, C.A. (2007) *Muscle Biopsy: A Practical Approach*. 3rd Ed. Saunders Elsevier, London, pp. 21–39.